

Cavitation on surfaces

This article has been downloaded from IOPscience. Please scroll down to see the full text article.

2005 J. Phys.: Condens. Matter 17 S3603

(<http://iopscience.iop.org/0953-8984/17/45/054>)

[The Table of Contents](#) and [more related content](#) is available

Download details:

IP Address: 155.69.4.4

The article was downloaded on 31/10/2009 at 16:44

Please note that [terms and conditions apply](#).

Cavitation on surfaces

Nicolas Bremond, Manish Arora, Claus-Dieter Ohl and Detlef Lohse

Physics of Fluids, University of Twente, PO Box 217, 7500 AE Enschede, The Netherlands

Received 3 October 2005

Published 28 October 2005

Online at stacks.iop.org/JPhysCM/17/S3603

Abstract

Entrapment of gas bubbles at the liquid/solid interface plays a crucial role for fluidic systems when the volume to surface ratio goes down. Here, we report an investigation on the presence of air on hydrophobic surfaces in water. The gas pockets on such walls are expanded, and thus made visible, by lowering the liquid pressure, a phenomenon known as heterogeneous cavitation. The investigation is extended to the study of the formation and the dynamics of bubbles generated from well controlled nuclei.

Introduction: gas on solid surfaces in water

The no-slip boundary condition of a liquid flowing over a solid surface seems to be violated in various experimental configurations [1, 2]. Since the boundary conditions play a major role once the volume/surface ratio of the system goes down, a better understanding of the liquid/solid features is necessary for microfluidic devices. The formation of a thin film of gas between the liquid and the solid has been proposed by de Gennes [3] to be responsible for this slippage. This point of view has been questioned as a result of ellipsometer measurements [4], but recent atomic force microscopy (AFM) investigations of solid surfaces underwater suggest the presence of softer objects with submicrometric sizes [5–8]. They have been interpreted as gas pockets and named nanobubbles but the reason for their apparent stability is still a mystery. Indeed, the inner pressure due to surface tension is inversely proportional to the bubble's radius, and should therefore lead to fast dissolution [9], making observation through AFM impossible.

Surface nanobubbles have also been observed in fast freezing experiments [10]. They can be involved in the liquid slippage over solid surfaces [11, 2] as they provide a quasi-zero-shear-stress interface. They could also play a role in the hydrophobic attraction between two particles resulting from nanobubble bridging [12, 13], or in thin film dewetting [14].

Since these bubbles are too small to be directly observed through optical microscopes, the idea of this work here is to expand them by decreasing the liquid pressure, i.e. through heterogeneous cavitation. In contrast, homogeneous nucleation is related to the breakdown of a pure liquid being stretched or heated up. A critical negative pressure of -140 MPa has been observed for ultrapure water at 42 °C [15]. In the present configuration, the gas pockets trapped on the solid surface initiate liquid fracture at much lower negative pressure or tensile strength.

We performed an investigation on the presence of gas on flat and smooth hydrophobic surfaces underwater using an acoustic wave with a minimum pressure reaching a few MPa.

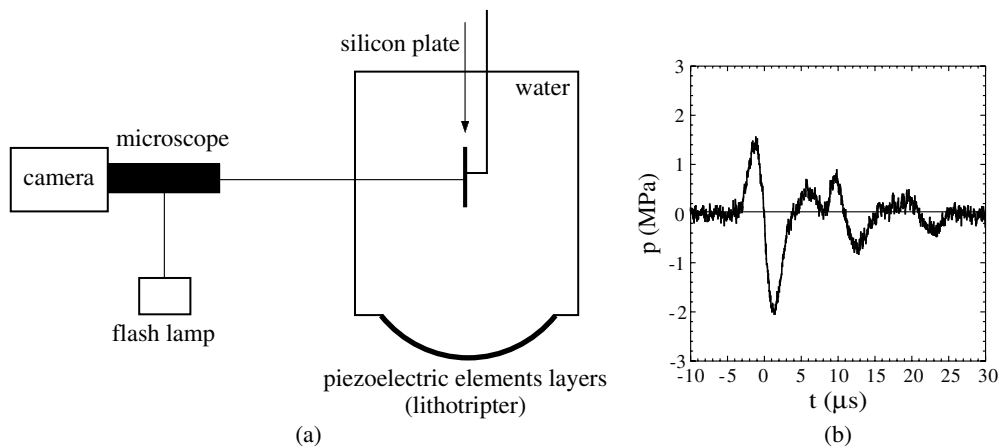


Figure 1. (a) Pressure wave generator and optical visualization. (b) Pressure signal recorded with an optical fibre [16].

This investigation is extended to the study of the formation and the dynamics of bubbles emerging from well controlled nuclei.

1. Experimental procedures

The experimental set-up is depicted in figure 1(a). A lithotripter device is used as pressure pulse generator and it is connected to a rectangular tank containing a litre of Milli-Q water saturated with gas at room temperature ($\sim 20^\circ\text{C}$). The device is made of two layers of piezoelectric components arranged on a portion of a sphere and driven by a high voltage discharge. The pressure signal p is recorded at the focus with an optical fibre (RP Acoustics, 2000 FOPH) by measuring the reflected intensity of the laser beam at the fibre tip which depends on the local impedance of the water changing as the pressure evolves [16]. An average of 50 events is reported in figure 1(b). The pressure wave is characterized by a high pressure front followed by a negative pressure pulse lasting $3\ \mu\text{s}$ and going down to around $-2\ \text{MPa}$. The substrates studied are fixed on a thin rod and placed at the focal point. The cavitation event is recorded with a charged coupled device (CCD) camera through a long working distance microscope. Motion blurring is minimized by a short exposure time of $0.2\ \mu\text{s}$.

Two kinds of samples have been used: plane surfaces with and without etched microcavities. Both are diced from a silicon wafer (100) and made hydrophobic as follows. The silicon wafer is cleaned and oxidized in a mixture of sulfuric acid and hydrogen peroxide before being coated with perfluorodecyltrichlorosilane (FDTS) by vapour deposition. After this procedure, the advancing contact angle of water has been measured to be $106^\circ \pm 1^\circ$. Prior to the silanization step, cylindrical cavities $15\ \mu\text{m}$ deep and from 2 to $4\ \mu\text{m}$ wide are etched on the wafer using the deep reactive ion etching (DRIE) technique. By employing this procedure, we ensure entrapment of air in these cavities during the immersion of the substrates in water.

2. Cavitation on a plane surface

According to homogeneous nucleation theory, cavitation results from the expansion of a spherical void with a radius R subjected to a negative pressure p (see [17] and references

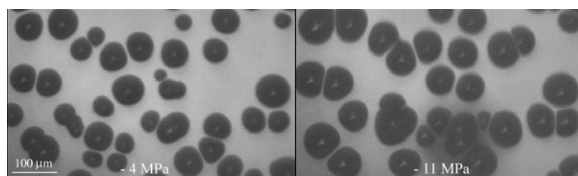


Figure 2. Snapshots of bubbles nucleated on a flat and smooth hydrophobic surface after the passage of pressure pulses with minimum pressures of -4 and -11 MPa. The cavitation events are observed from above on the same substrate and at the same location.

within). The total pressure inside the bubble p_i , i.e. the vapour pressure p_v plus the gas pressure p_g , is connected to the external pressure p via Laplace's equation, $p_i = p_v + p_g = p + 2\sigma/R$. Once p becomes too small, the bubble is mechanically unstable and grows explosively.

Heterogeneous cavitation takes place from solid particles present in the bulk, or on the walls of the vessel containing the liquid. The nuclei are assumed to be stabilized in small crevices allowing a modification of the interface curvature preventing them from dissolution [18, 19]. For a given gas concentration, the stabilization depends on the wetting properties of the liquid on the solid surface and the geometry of the crevices. Nanobubbles have been observed on smooth and flat substrates as silicon wafers [8] without such stabilizing cavities. We have thus studied cavitation occurring on the same kinds of solid surfaces.

We use hydrophobic silicon plates with a mean roughness less than 2 nm as measured with an AFM (PicoSPM). Figure 2 presents two snapshots of the nucleation of bubbles on such surfaces after the passage of negative pressure waves with pressures of -4 and -11 MPa. The corresponding minimal radii probed by these negative pressures are 37 and 13 nm, respectively. The pictures are taken at the same location and the substrate is rinsed with ethanol and blown with nitrogen before each immersion in the water. This cleaning procedure ensures a quick drying of the surface. We first notice that the density of cavitating bubbles is quite similar from one experiment to another. The minimum radius of the nuclei sitting on the solid surface is thus larger than 37 nm.

Next, we observe some preferential sites of nucleation, which are also seen when performing the experiment at the same pressure level. This observation suggests that gas is trapped on localized defects or contaminants during the wetting step. Indeed, a geometrical or chemical defect can pin the triple contact line as it moves on the surface and entraps air [20]. In order to confirm this hypothesis, a thin film of ethanol is left on the surface preventing direct contact with air. In this case, a lowering of the liquid pressure does not lead to cavitation on the substrate.

Such nuclei are not stable over time for ambient conditions. The density of bubbles (number per unit area) decreases by a factor of ten if we wait two hours between the immersion time and the pressure pulse loading ('shot'). The bubbles shrink by gas diffusion through the interface due to the larger internal gas pressure. Indeed, the equilibrium gas concentration in a liquid is proportional to the partial gas pressure at a free surface, leading to a gas concentration gradient between the region near the bubbles and the bulk [9].

It has also been noticed that the density of cavitating bubbles is a decreasing function of the number of successive shots when the substrate is kept in water. The density drops down by a factor of ten after 50 shots, but some nucleation events occur even after more than several hundred shots. This continued occurrence of cavitation events could be due to the formation of submicron bubbles from the collapse of the cavitating bubbles [21], acting as nuclei for the following pressure wave.

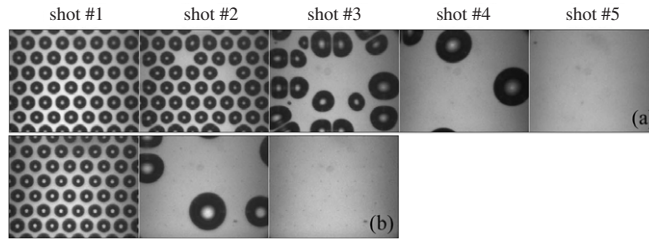


Figure 3. Cavitation occurrence from a regular array of hydrophobic cavities with a diameter of $2\ \mu\text{m}$ (a) and $4\ \mu\text{m}$ (b) after successive low pressure pulses with minimum pressure of $-2\ \text{MPa}$.

3. Cavitation from controlled nuclei and bubble dynamics

We now use the substrates with etched microcavities in which gas is trapped prior to the plate immersion in water. These gas pockets expand after the passage of the negative pressure pulse and can reach a size of the order of a hundred times their initial size and then finally collapse after a few tens of microseconds. They are found to be stable against dissolution. Indeed, if the negative pressure pulse is not applied until 15 h of immersion have elapsed, each cavity still nucleates a bubble. This behaviour is due to the sharp edge of the hydrophobic cavity which can sustain a flat liquid/gas interface. Without forcing, the gas pressure is thus equal to the ambient gas pressure in the liquid preventing gas diffusion through the bubble surface.

On the other hand, the cavities do not nucleate bubbles any longer after a number of successive shots; all the gas is released in the water after a few cavitation events. This is reported in figure 3 for two cavity diameters, $2\ \mu\text{m}$ and $4\ \mu\text{m}$, where the minimum pressure is $-2\ \text{MPa}$. We notice that the smaller the cavity diameter, the larger the number of shots needed for removing all the entrapped air. This observation suggests that the bubbles nucleated on the smooth solid surface (figure 2) start from very small nuclei, as they are still generated after several tens of shots. Bubbles are also nucleated on the smooth part of the patterned surface at this pressure level, but their density is lower than previously and the uncontrolled nuclei are not activated any longer if the surface is not dried in the same way as for the experiments described in section 2.

The complete history of a cavitating bubble can be followed by changing the time delay between the couple flash/camera. The substrate is pulled off the water tank and plunged again for ensuring air entrapment in the cavities between two recordings. Two snapshots of a single bubble and a pair of bubbles are displayed in figures 4(a) and (b). The evolution of the radius $R(t)$ of an isolated bubble is plotted in figure 4(c) as a function of time. The cavity filled with air is exposed to the pressure wave shown in figure 1(b). The vertical bars represent the standard deviation obtained for several runs. This variation is due to some pressure fluctuations between shots. The radius dynamics is nicely reproducible during the expansion phase but the variation increases near the collapse.

The dynamics of this hemispherical bubble is ruled by the Rayleigh–Plesset equation if we neglect the wall effect and assume an analogy with half of a free bubble [22, 23]:

$$R\ddot{R} + \frac{3}{2}\dot{R}^2 = \frac{1}{\rho} \left(p_i - p_\infty(t) - \frac{2\sigma}{R} - \frac{4\mu}{R}\dot{R} + \frac{R}{c} \frac{dp_i}{dt} \right) \quad (1)$$

where ρ is the liquid density, σ the surface tension, μ the dynamic viscosity of the liquid, p_i the pressure in the bubble and $p_\infty(t)$ the pressure of the liquid at large distance from the bubble. The pressure $p_\infty(t)$ is determined as the mean of several experimental pressure recordings as shown in figure 1(b). The numerical integration of equation (1) gives the evolution of $R(t)$ as

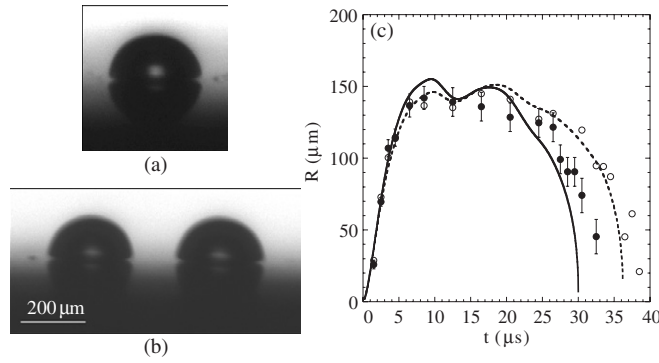


Figure 4. Side view of a single expanding bubble on a solid surface (a), and two bubbles initially $400 \mu\text{m}$ apart (b). The length scales on the two pictures are the same and the snapshots correspond to $t = 8.5 \mu\text{s}$. (c) Evolution of the bubble radius versus time for a single cavity (●) and two cavities $400 \mu\text{m}$ apart (○). The curves are the theoretical predictions given by equations (1) (continuous line) and (2) (dashed line).

displayed in figure 4(c). The Rayleigh–Plesset equation describes the evolution of the bubble’s radius well during the expansion phase, but predicts too fast a collapse. It is worth mentioning that the present analysis breaks down close to the collapse for strong forcing [23, 24].

Two bubbles cavitating close to each other will interact as they modify the surrounding liquid pressure during their expansion and collapse. The mean radius of two bubbles with centres $400 \mu\text{m}$ apart is plotted in figure 4(c). We notice that the bubble pair lasts longer than the isolated bubble. Since the distance d between the two cavities is only a few hundreds of microns, we can assume an instantaneous evolution of the pressure (not retarded, i.e. infinite sound velocity) and uniformly distributed around each bubble. The dynamics of the two bubbles are identical since the median plane between them is a plane of symmetry. On taking into account the pressure field generated by the neighbouring bubble deduced from the integration of the Navier–Stokes equation from r to ∞ , the Rayleigh–Plesset equation is modified as follows (see e.g. [25]):

$$R\ddot{R} + \frac{3}{2}\dot{R}^2 = \frac{1}{\rho} \left(p_i - p_\infty(t) - \rho \frac{R}{d} (R\ddot{R} + 2\dot{R}^2) - \frac{2\sigma}{R} - \frac{4\mu}{R} \dot{R} + \frac{R}{c} \frac{dp_i}{dt} \right). \quad (2)$$

The radius evolution predicted by equation (2) for $d = 400 \mu\text{m}$ is plotted in figure 4(c) and compared with the experimental data. The pressure coupling is apparently sufficient for the description of the bubble interaction. This study will be extended to multibubble interaction such as happens in clusters occurring in many industrial configurations and which is responsible for structure damages [17].

We have summarized here our work on cavitation on hydrophobic surfaces in water. The nucleation of bubbles takes place on initially smooth surfaces for negative pressures much smaller than the pressure threshold of water rupture. The cavitation bubbles emerge from unstable nuclei which are found to be trapped during the step of wetting of the solid surfaces. The dynamics and the interactions of such expanding bubbles are studied finally, with the help of well controlled cavities acting as gas traps. A good agreement is found between the experimental behaviour of cavitating bubbles on a solid surface and that predicted by the Rayleigh–Plesset approach.

Acknowledgments

We acknowledge Han Gardeniers for providing us the substrates and Pascale Maury for sharing with us some chemical recipes.

References

- [1] Granick S, Zhu Y and Lee H 2003 *Nat. Mater.* **2** 221
- [2] Lauga E, Brenner M P and Stone H A 2005 *Handbook of Experimental Fluid Dynamics* (Berlin: Springer)
- [3] de Gennes P G 2002 *Langmuir* **18** 3413
- [4] Mao M, Zhang J, Yoon R H and Ducker W A 2004 *Langmuir* **20** 1843
- [5] Ishida N, Inoue T, Miyahara M and Higashitani K 2000 *Langmuir* **16** 6377
- [6] Tyrrell J W G and Attard P 2001 *Phys. Rev. Lett.* **87** 176104
- [7] Holmberg M, Kuhle A, Garnaes J, Morch K A and Boisen A 2003 *Langmuir* **19** 10510
- [8] Yang J, Duan J, Fornasiero D and Ralston J 2003 *J. Phys. Chem. B* **107** 6139
- [9] Epstein P S and Plesset M S 1950 *J. Chem. Phys.* **18** 1505
- [10] Switkes M and Ruberti J W 2004 *Appl. Phys. Lett.* **84** 4759
- [11] Lauga E and Stone H A 2003 *J. Fluid Mech.* **489** 55
- [12] Attard P 2003 *Adv. Colloid Interface Sci.* **104** 75
- [13] Evans D R, Craig V S J and Senden T J 2004 *Physica A* **339** 101
- [14] Stockelhuber K W, Radoev B, Wenger A and Schulze H J 2004 *Langmuir* **20** 164
- [15] Zheng Q, Durben D J, Wolf G H and Angell C A 1991 *Science* **254** 829
- [16] Staudenraus J and Eisenmenger W 1993 *Ultrasonics* **31** 267
- [17] Brennen C E 1995 *Cavitation and Bubble Dynamics* (Oxford: Oxford University Press)
- [18] Harvey E N, Barnes D K, McElroy W D, Whiteley A H, Pease D C and Cooper K W 1944 *J. Cell. Comp. Physiol.* **24** 1
- [19] Atchley A A and Prosperetti A 1989 *J. Acoust. Soc. Am.* **86** 1065
- [20] de Gennes P G 1985 *Rev. Mod. Phys.* **57** 827
- [21] Yavas O, Leiderer P, Park H E, Grigoropoulos C P, Poon C C and Tam A C 1994 *Phys. Rev. Lett.* **72** 2021
- [22] Plesset M S and Prosperetti A 1977 *Annu. Rev. Fluid Mech.* **9** 145
- [23] Prosperetti A and Lezzi A 1986 *J. Fluid Mech.* **168** 457
- [24] Brenner M P, Hilgenfeldt S and Lohse D 2002 *Rev. Mod. Phys.* **74** 425
- [25] Harkin A, Kaper T J and Nadim A 2001 *J. Fluid Mech.* **445** 377